

Accepted by ApJ at August 21, 2014.

Induced Core Formation Time in Subcritical Magnetic Clouds by Large-Scale Trans-Alfvénic Flows

Takahiro Kudoh¹

*Division of Theoretical Astronomy, National Astronomical Observatory of Japan, 2-21-1
Osawa, Mitaka, Tokyo 181-8588, Japan*

kudoh@th.nao.ac.jp

and

Shantanu Basu

*Department of Physics and Astronomy, University of Western Ontario, London, Ontario
N6A 3K7, Canada*

basu@uwo.ca

ABSTRACT

We clarify the mechanism of accelerated core formation by large-scale non-linear flows in subcritical magnetic clouds by finding a semi-analytical formula for the core formation time and describing the physical processes that lead to them. Recent numerical simulations show that nonlinear flows induce rapid ambipolar diffusion that leads to localized supercritical regions that can collapse. Here, we employ non-ideal magnetohydrodynamic simulations including ambipolar diffusion for gravitationally stratified sheets threaded by vertical magnetic fields. One of the horizontal dimensions is eliminated, resulting in a simpler two-dimensional simulation that can clarify the basic process of accelerated core formation. A parameter study of simulations shows that the core formation time is inversely proportional to the square of the flow speed when the flow speed is greater than the Alfvén speed. We find a semi-analytical formula that explains this numerical result. The formula also predicts that the core formation time is about three times shorter than that with no turbulence, when the turbulent speed is comparable to the Alfvén speed.

¹Department of Astronomical Science, School of Physical Sciences, the Graduate University for Advanced Studies (SOKENDAI), 2-21-1 Osawa, Mitaka, Tokyo 181-8588, Japan

Subject headings: ISM: clouds — ISM: magnetic fields — stars: formation

1. Introduction

The theory that the star formation process in a molecular cloud is controlled by the magnetic field and ambipolar diffusion has been studied for many years (e.g., Mouschovias 1978; Shu et al. 1987). In the theory, the mass-to-flux ratio, which corresponds to the relative strength of gravity and the magnetic field, is an important parameter for the process. If the mass-to-flux ratio is greater than its critical value (i.e., supercritical : gravity dominates the magnetic field), the cloud is likely to collapse or fragment on the dynamical timescale. If the mass-to-flux ratio is less than its critical value (i.e., subcritical : the magnetic field dominates gravity), the gravitational driven collapse or fragmentation occurs on the ambipolar diffusion timescale (e.g., Langer 1978; Zweibel 1998) instead of the dynamical timescale as long as the diffusion timescale is longer than the dynamical timescale. Although there are some observational difficulties to determine whether the mass-to-flux ratio of molecular clouds are greater or lesser than the critical value prior to core formation (e.g. Crutcher et al. 2009; Mouschovias & Tassis 2009), subcritical molecular clouds are consistent with some observations that show that molecular clouds are associated with large-scale ordered magnetic fields (e.g., Cortes et al. 2005; Heyer et al. 2008; Alves et al. 2008; Li et al. 2009).

Here, we focus on fragmentation and core formation in subcritical molecular clouds. The first numerical simulations of fragmentation in subcritical clouds with ambipolar diffusion were performed by Indebetouw & Zweibel (2000) under the assumption of a two-dimensional infinitesimally thin sheet. Basu & Ciolek (2004) carried out simulations of magnetized sheets including the effect of a finite disk half-thickness that was consistent with hydrostatic equilibrium. A three-dimensional simulation of fragmentation and core formation in subcritical clouds with ambipolar diffusion, including full gravitational stratification along the magnetic field, was first performed by Kudoh et al. (2007). These numerical calculations confirmed that the gravitationally driven fragmentation and core formation in subcritical clouds occur on the ambipolar diffusion timescale. Core formation in subcritical clouds generally explains the low star formation rate in our galaxy, since the typical ambipolar diffusion time is more than 10 times longer than the dynamical time in molecular clouds. On the other hand, a problem has been pointed out that the ratio of starless and stellar cores is smaller than that is expected from the theory (e.g., Jijina et al. 1999). The observations mean that core formation is likely to occur on up to several dynamical times, i.e., the usual ambipolar diffusion time is about 3 – 10 times longer than that expected from the observations.

Ideas to solve the timescale problem were proposed by Fatuzzo & Adams (2002), who pointed out that fluctuating magnetic fields and density in turbulent molecular clouds can enhance the ambipolar diffusion rate because the ambipolar diffusion is a process of nonlinear diffusion. Their analysis indicated that the density fluctuation enhances the diffusion rate more efficiently when the amplitude of the fluctuation is large. Their idea is consistent with the fact that supersonic turbulence is considered to be a significant factor in molecular clouds as well as for magnetic fields during the early stage of star formation (e.g., McKee & Ostriker 2007), since the supersonic turbulence tends to enhance the density through compression. Li & Nakamura (2004) carried out numerical simulations of fragmentation in subcritical clouds with a thin-sheet approximation, including both ambipolar diffusion and supersonic turbulent flow. They found that the timescale of core formation in subcritical clouds is reduced by the supersonic turbulent flow as long as the turbulence is dominated by large-scale fluctuations. Basu et al. (2009) confirmed the fast core formation by nonlinear large-scale turbulent flows with a numerical simulation using the thin-sheet approximation. They also found that the subcritical clouds experienced rebounds after the first compression and showed several oscillations before the core formation as long as the initial flow speed is trans-Alfvénic. These results were also confirmed by Kudoh & Basu (2008) and Kudoh & Basu (2011) through three-dimensional simulations without the thin-sheet approximation. Kudoh & Basu (2011) found that the core formation time (t_{core}) roughly scales as $t_{core} \propto \rho_{peak}^{-0.5}$, where ρ_{peak} represents the first density peak created by the compression induced by the supersonic turbulent flow. Kudoh & Basu (2011) also confirmed that the core formation time is shorter when the turbulent flow speed is greater. Although these results indicate that the density enhancement in subcritical clouds is an important factor to shorten the core formation time, they did not clarify the physical process of how the density enhancement shortens the core formation time as well as how the core formation time depends on the turbulent flow speed. This motivates us to carry out further investigations of the induced core formation by nonlinear flows in subcritical clouds. Previous studies indicated that large-scale compression would be the key process to enhance the ambipolar diffusion rate. In this short paper, we present the investigation of the core formation under a simple large-scale nonlinear flow rather than complex turbulent flows. We study basic properties of the core formation in subcritical clouds to achieve a clear explanation of how the fast ambipolar diffusion is induced by large-scale compression in the clouds.

This paper is organized as follows. We have a brief description of the setup for numerical simulations in Section 2. The numerical results and its semi-analytical explanation are given in Section 3. We summarize the results and have some discussions in Section 4.

2. Setup for Numerical Simulation

The numerical setup in this paper is similar to that used in Kudoh & Basu (2011), but spatial symmetry is assumed in one of the directions perpendicular to the magnetic field. We effectively solve the magnetohydrodynamic (MHD) equations in two spacial dimensions with self-gravity and ambipolar diffusion. The equation for the time evolution of the magnetic field with ambipolar diffusion is assumed to be the one-fluid model as

$$\frac{\partial \mathbf{B}}{\partial t} = \nabla \times (\mathbf{v} \times \mathbf{B}) + \nabla \times \left[\frac{\gamma}{4\pi\rho^{3/2}} (\nabla \times \mathbf{B}) \times \mathbf{B} \right], \quad (1)$$

where \mathbf{B} is the magnetic field, \mathbf{v} is the velocity, ρ is the density of neutral gas, $\gamma \simeq 170.2 \text{ g}^{1/2}\text{cm}^{-3/2} \text{ s}$ is used as the typical value in molecular clouds (e.g., Basu & Mouschovias 1994). In the two-dimensional Cartesian coordinate system (x, z) , the initial magnetic field is assumed to be uniform along the z -direction:

$$B_z = B_0, \quad B_x = 0, \quad (2)$$

where B_x and B_z are the magnetic field components of the x - and z -directions, respectively, and B_0 is constant. In this coordinate system, we assume physical variables are constant along the direction perpendicular to both the x - and z -directions.

The initial hydrostatic equilibrium of a self-gravitating cloud along the magnetic field (z -direction) is assumed. If the temperature of the cloud is uniform throughout the region, the analytic density distribution ρ_S was obtained by Spitzer (1942):

$$\rho_S(z) = \rho_0 \text{sech}^2(z/H_0), \quad (3)$$

where

$$H_0 = \frac{c_{s0}}{\sqrt{2\pi G \rho_0}}, \quad (4)$$

ρ_0 is the density at $z = 0$, c_{s0} is the sound speed, and G is the gravitational constant. Instead of the uniform temperature, we use the hyperbolic tangent function for temperature distribution that shows a sharp transition from low temperature to 10 times higher temperature around $z = 2H_0$ (see Kudoh & Basu 2011). This function mimics the situation that warm gas commonly surrounds the isothermal molecular cloud. The initial hydrostatic density distribution obtained from the temperature distribution is almost the same as that of equation (3) in the low temperature region in which we are interested. We model molecular clouds in the number density range $10^3 \text{ cm}^{-3} - 10^6 \text{ cm}^{-3}$. Since the cooling time is much shorter than the dynamical time in this density range, we adopt isothermality for each Lagrangian fluid element (Kudoh & Basu 2003, 2006).

In the sheet we mimic the largest mode of a turbulent flow with an initial sinusoidal velocity fluctuation along the x -direction:

$$v_x = -v_{max} \sin(2\pi x/x_{max}) \quad (\text{if } |x| \leq 0.5x_{max}), \quad (5)$$

where v_x is the velocity component of x -direction, v_{max} is the velocity amplitude of the fluctuation and a variable parameter in this work, and x_{max} is fixed to equal $4\pi H_0$ throughout the paper. The most unstable wavelength of gravitational instability is about $4\pi H_0$ in the case with no magnetic field (Miyama et al. 1987a), and the corresponding wavelength with magnetic field is expected to be close to $4\pi H_0$ unless the cloud is marginally critical (Ciolek & Basu 2006). Due to this sinusoidal velocity fluctuation, the initial flow converges the cloud toward $x = 0$. Since the symmetry is assumed in the direction perpendicular to the x - and z -directions, the converging flow makes a filamentary structure rather than a spherical one. In the previous three-dimensional simulations of large-scale turbulent flows with energy spectrum of k^{-4} (Kudoh & Basu 2011), where k is the wave number of the turbulence, a similar filamentary structure is produced in the cloud before the gravitational fragmentation. The sinusoidal velocity fluctuation is a simple model to simulate the fragmentation and collapse in a large-scale turbulent flow.

As units for this problem, H_0 , c_{s0} , and ρ_0 are chosen for length, velocity, and density, respectively. These give a time unit $t_0 \equiv H_0/c_{s0}$. The strength of the initial magnetic field brings one dimensionless free parameter,

$$\beta_0 \equiv \frac{8\pi\rho_0 c_{s0}^2}{B_0^2}. \quad (6)$$

The parameter β_0 represents the initial ratio of gas to magnetic pressure at $z = 0$, and has a relation with μ_S as

$$\beta_0 = \mu_S^2, \quad (7)$$

where μ_S is the the mass-to-flux ratio normalized to the critical value of the cloud whose density distribution is described by equation (3) (see Kudoh & Basu 2011). Since we are interested in subcritical clouds, we take β_0 values less than 1 in this paper. Dimensional values can be obtained by specifying ρ_0 and c_{s0} . In the case of $c_{s0} = 0.2 \text{ km s}^{-1}$ and $n_0 = \rho_0/m_n = 10^4 \text{ cm}^{-3}$ where $m_n = 2.33 \times 1.67 \times 10^{-24} \text{ g}$, we obtain $H_0 \simeq 0.05 \text{ pc}$, $t_0 \simeq 2.5 \times 10^5 \text{ year}$, and $B_0 \simeq 40 \mu\text{G}$ if $\beta_0 = 0.25$.

The numerical methods are based on those of Ogata et al. (2004) for solving the MHD equations and Miyama et al. (1987b) for solving the self-gravity. The calculating area is taken to be $-4\pi H_0 \leq x \leq 4\pi H_0$ and $0 \leq z \leq 4H_0$. The number of grid points is 256 for the x -direction and 40 for the z -direction. A mirror-symmetric boundary at $z = 0$ and

periodic boundaries in the x -directions are used. A mirror-symmetric boundary is also used at the upper boundary ($z = 4H_0$) for convenience except for the gravitational potential (see details and discussion in Kudoh & Basu (2011)). As it was done before (Kudoh et al. 2007; Kudoh & Basu 2008, 2011), the ambipolar diffusion term is assumed to work only when the density exceeds a certain value, $\rho_{cr} = 0.3\rho_0$ to prevent small time steps occurring outside of the low temperature cloud.

3. Numerical Results and Semi-Analytical Formulation

3.1. Parameters

The summary of the models and parameters for the simulations are given in Table 1. In this table, the values of the free parameters β_0 and v_{max} are listed. The parameter v_{max} is listed both normalized by the sound speed c_{s0} and the initial Alfvén speed v_{A0} on the midplane ($z = 0$) of the clouds, where $v_{A0} = B_0/\sqrt{4\pi\rho_0}$. The core formation time t_{core} , which is characterized as the time when the maximum density attained $100\rho_0$, is also listed. The definition of t_{core} is the same as that in Kudoh & Basu (2011). Although t_{core} is defined from a practical restriction of the numerical simulation, the center of the core always showed the features of runaway collapse at that time. In the models A003 to A10, the amplitude of the initial velocity fluctuation v_{max} is changed with the fixed $\beta_0 = 0.25$. In the models B01 to B15, v_{max} is changed with the fixed $\beta_0 = 0.09$. In the models C1 to C7, v_{max} is also changed with the fixed $\beta_0 = 0.49$. In the models D3 to D15, v_{max} is changed with a fixed $\beta_0 = 0.04$. In addition to these models, the model E5 is also introduced, with the same parameters as those of model A5 except that the ambipolar diffusion is artificially switched off.

3.2. General Properties

In Figure 1, the snapshot of the logarithmic density for the model A5 is shown as a color map, when the maximum density becomes greater than a hundred times of the initial density. The vectors overlaid in Figure 1 indicate the velocity. Since the initial flow converges the cloud toward $x = 0$, the figure shows that a collapsing core is located at the origin of the coordinate. The shape of the core is approximately oblate whose apse line is along the x -direction in spite of the converging flow. This is because the core formation does not occur during the first compression, but it occurs gradually in the oscillating cloud. We will see this process in Figure 5 later. The logarithmic plasma β (the ratio of gas pressure to magnetic

pressure) for the model A5 is shown in Figure 2 at the same time as that of Figure 1. Figure 2 shows that β is greater than 1 near the center of the core, though the initial β is 0.25 on $z = 0$ ($\beta_0 = 0.25$). It means that the magnetic flux has been removed from the core and the mass-to-flux ratio of the collapsing core is expected to be greater than 1 (see equation 7), i.e., the core is supercritical around the center. We will see this feature again in the following discussion.

Figure 3 shows the snapshot ($t = 24.5t_0$) of the spatial profiles of density, magnetic field strength, and x-velocity along x on $z = 0$ for the model A5. Both the density and magnetic field have peaks at $x = 0$ where the flow converges. The flow remains large scale and does not become turbulent in this simulation. Figure 4 shows the snapshot ($t = 24.5t_0$) of spatial profiles of surface density (Σ_N) and normalized mass-to-flux ratio (μ_N) along x for the same model A5. They are conventionally defined in the following equations:

$$\Sigma_N \equiv \int_{-z_B}^{z_B} \rho dz, \quad (8)$$

$$\mu_N \equiv 2\pi G^{1/2} \frac{\Sigma_N}{|B_z(z=0)|}, \quad (9)$$

where $z_B = 4H_0$ is the upper boundary value in the calculating area, and $B_z(z=0)$ is the z component of the magnetic field at $z = 0$. The normalized mass-to-flux ratio is greater than 1 near the peak of the surface density. This means that the region has evolved from a subcritical to supercritical state through the removal of magnetic flux. In Figure 4, the square root of plasma β at $z = 0$ is also plotted. It shows that $\beta^{1/2}$ follows a similar profile as that of the normalized mass-to-flux ratio, and β is nearly greater than 1 where μ_N is greater than 1. Since β is locally defined in the simulation, it is convenient to use β as an approximate indicator of the magnetic criticality of the cloud, although it is not exactly the same as μ_N .

Figure 5 shows the time evolution of the density at the location of the core center (ρ_c), i.e., $(x, z) = (0, 0)$. The solid line shows the case of model A5. The density increases during the first compression of the cloud. Next, it bounces and undergoes oscillations. Finally, the dense region goes into runaway collapse after $t/t_0 \sim 20$. Figure 6 shows the time evolution of β at the the core center (β_c). In the very initial stage of the compression ($t/t_0 < 1$), β_c rapidly decreases, but it increases soon as the density reaches a peak around $t/t_0 \sim 1$. After that, it decreases and shows oscillations as seen in the time evolution of the density. Eventually, it gradually increases with oscillations and becomes greater than 1 when the runaway collapse happens. Since β_c approximately equals the square of the mass-to-flux ratio, the runaway collapsing core is expected to be supercritical. Figure 6, as well as Figure

2 and Figure 4, shows that β_c can be a good indicator of the mass-to-flux ratio during the oscillations, even though the gravitational equilibrium of the gas is not exactly established at the final stage of the simulation. The first rapid decrease of β_c ($t/t_0 < 1$) could be a result of the non-equilibrium of the gas along the magnetic field. The dotted lines in Figures 5 and 6 show the case of model E5 in which the parameters are the same as those of model A5 except that the ambipolar diffusion is artificially switched off. When the ambipolar diffusion is switched off, the density and β_c do not show the feature of collapse while they do show oscillations. This also indicates that the collapse is caused by the removal of the magnetic flux through the ambipolar diffusion. In Figures 5 and 6, the dashed lines show the case of model A3 whose initial converging flow speed is smaller than that of model A5, and dotted-dashed lines show the case of the model A10 whose initial flow speed is larger than that of the model A5. The overall features of the time evolutions are qualitatively similar, though the core formation time is shorter when the initial flow speed is greater. When the initial flow speed is high enough (for the model A10), β_c becomes greater than 1 at the first peak. In that case, it rebounds a little bit, but goes into runaway collapse very soon.

3.3. Core Formation Time

Figure 7 shows the core formation time as a function of the initial flow speed v_{max} . The flow speed is normalized by the sound speed. The filled circles show the case of $\beta_0 = 0.25$ (the models A003 to A10). The open squares show the case of $\beta_0 = 0.09$ (the models B01 to B15). The open triangles show the case of $\beta_0 = 0.49$ (the models C1 to C7). The filled triangles show the case of $\beta_0 = 0.04$ (the models D3 to D15). As the flow speed increases, the core formation time decreases for each set of β_0 values. The case of the smaller β_0 , i.e., the smaller initial mass-to-flux ratio, shows a longer core formation time for the same initial flow speed. The flow speed normalized by the sound speed may be useful when the results are compared with observations. On the other hand, in figure 8, we plot the core formation time as a function of v_{max} , like in figure 7, but normalized by the initial Alfvén speed on the midplane of the clouds (v_{A0}). In figure 8, all results fall on the same line regardless of the value of β_0 . The core formation time is approximately the same for the same initial flow speed if it is normalized by the Alfvén speed. The dashed line shows the semi-analytic result which is obtained in the next subsection. The core formation time is in inverse proportion to the square of v_{max} , when v_{max} is greater than v_{A0} . We will have a detailed discussion of this result in the next subsection.

The core formation time is also shown in figure 9 as a function of ρ_{peak} , defined as the value of the density peak during the first compression in the time evolution of the central

density at $x = 0$ and $z = 0$. As we have discussed in our previous paper (Figure 16 in Kudoh & Basu (2011)), the core formation time is proportional to $\rho_{peak}^{-0.5}$ when ρ_{peak}/ρ_0 is enough greater than 1. The dashed line shows the semi-analytic result obtained in the next subsection, which shows $t_{core} \propto \rho_{peak}^{-0.5}$. Figure 9 shows the relation clearly, and the figure also indicates that the relation does not depend on β_0 , i.e., the initial mass-to-flux ratio. The result is also discussed in the next subsection in detail.

3.4. Semi-Analytical Formulation

In this subsection, we find the semi-analytical formulas of core formation time and compare them with the numerical results in the previous subsections. Since figure 5 and figure 6 shows the oscillation of the cloud, we considered the cloud to be in an approximate force balance for a time average of the period. When we assume force balance between the magnetic force and gravity along the x -axis in the cylindrical subcritical cloud (Mouschovias & Ciolek 1999),

$$\rho \frac{GM_l}{L} \sim \frac{B^2}{8\pi} \frac{1}{L}, \quad (10)$$

where

$$M_l \sim \pi H L \rho \quad (11)$$

is the line mass along the cylinder, L is the half-size of the cloud in the x -direction, and H is the half thickness of the cloud in z -direction. The magnetic field is derived from these two equations as

$$B^2 \sim 8\pi\rho GM_l \sim 8\pi^2 G \rho^2 H L. \quad (12)$$

From the equation (1), the ambipolar diffusion time (τ_{AD}) is estimated to be

$$\tau_{AD} \sim \frac{4\pi}{\gamma} \frac{L^2 \rho^{3/2}}{B^2} \sim \frac{1}{2\pi\gamma G} \frac{L}{H} \rho^{-1/2}. \quad (13)$$

Since the most unstable wave length of the subcritical cloud is about $4\pi H$, we take

$$L \sim 4\pi H \times \frac{1}{2}. \quad (14)$$

Therefore, we get

$$\tau_{AD} \sim \frac{1}{\gamma G} \rho^{-1/2}. \quad (15)$$

This is the same equation that was derived in Mouschovias & Ciolek (1999). Although we derive it for cylindrical clouds, the result does not depend on the geometry of the cloud.

The dashed line in figure 9 is drawn from the equation (15), when we use $\rho \sim \rho_{peak}$ approximately. The figure 9 shows that the scaling relation agrees with the result of the numerical simulations. The relation also indicates that it does not depend on the initial mass-to-flux ratio.

Next, we consider the local pressure balance during the compression by the large scale flows. Since the cloud is subcritical, the thermal pressure can be negligible. Then, the pressure balance along x axis will be

$$H \frac{B^2}{8\pi} \sim H_0 \left(\rho_0 v_{t0}^2 + \frac{B_0^2}{8\pi} \right), \quad (16)$$

where v_t is the nonlinear flow speed in the cloud and the subscripts 0 mean the values before the compression. When we assume that there is sufficient time for the vertical density structure to be put back into hydrostatic equilibrium, i.e., $t/t_0 > 1$, H is estimated to be

$$H \sim \frac{c_s}{\sqrt{2\pi G \rho}}. \quad (17)$$

Therefore, the equation (16) becomes

$$\frac{1}{\sqrt{\rho}} \frac{B^2}{8\pi} \sim \frac{1}{\sqrt{\rho_0}} \left(\rho_0 v_{t0}^2 + \frac{B_0^2}{8\pi} \right), \quad (18)$$

in the isothermal gas, and this leads to

$$\left(\frac{\rho}{\rho_0} \right)^{1/2} \sim \left(v_{t0}^2 + \frac{B_0^2}{8\pi \rho_0} \right) \left(\frac{B^2}{8\pi \rho} \right)^{-1}. \quad (19)$$

When the ambipolar diffusion time is longer than the compression time, flux-freezing can be a good approximation during the compression, i.e.,

$$\frac{B}{\Sigma} \sim \frac{B_0}{\Sigma_0}, \quad (20)$$

where Σ is the surface density. Since $\Sigma \sim 2\rho H$, equation (20) is compatible with

$$\frac{B}{\rho^{1/2}} \sim \frac{B_0}{\rho_0^{1/2}} \quad (21)$$

in our approximation. Finally, equation (19) then becomes

$$\left(\frac{\rho}{\rho_0} \right)^{1/2} \sim 2 \left(\frac{v_{t0}}{v_{A0}} \right)^2 + 1, \quad (22)$$

where

$$v_{A0}^2 = \frac{B_0^2}{4\pi\rho_0} \quad (23)$$

is the square of the Alfvén speed of the cloud. By using this equation, the equation for the ambipolar diffusion time (15) is expressed using the flow speed as

$$\tau_{AD} \sim \frac{1}{\gamma G} \rho_0^{-1/2} \left[2 \left(\frac{v_{t0}}{v_{A0}} \right)^2 + 1 \right]^{-1}. \quad (24)$$

The dashed line in figure 6 is drawn from the equation (24), when we use $v_{t0} \sim 0.5v_{max}$ as an average speed. The figure 6 shows that the scaling relation agrees with the results of the numerical simulations. When the flow speed is comparable to the Alfvén speed, the ambipolar diffusion time is estimated to be

$$\tau_{AD} \sim \frac{1}{3} \frac{1}{\gamma G} \rho_0^{-1/2}, \quad (25)$$

which means the the ambipolar diffusion time is about three times shorter than that without the disturbance. When the flow speed is greater than the Alfvén speed,

$$\tau_{AD} \propto v_{t0}^{-2}, \quad (26)$$

which means that the ambipolar diffusion time is inversely proportional to the square of the nonlinear flow speed in a subcritical magnetic cloud.

4. Summary and Discussion

Since the core formation time (t_{core}) is almost comparable to the ambipolar diffusion time in a subcritical magnetic cloud, the relations

$$t_{core} \sim \tau_{AD} \sim \frac{1}{\gamma G} \rho^{-1/2}, \quad (27)$$

and

$$t_{core} \sim \tau_{AD} \sim \frac{1}{\gamma G} \rho_0^{-1/2} \left[2 \left(\frac{v_{t0}}{v_{A0}} \right)^2 + 1 \right]^{-1} \quad (28)$$

are consistent with the results of the numerical simulations in figure 8 and figure 9 as long as the turbulent velocities (v_{t0}) are large enough to compress the cloud, using $\rho \sim \rho_{peak}$ as a representative density and $v_{t0} \sim 0.5v_{max}$ as an average speed. When the observed turbulent speed is comparable to the Alfvén speed, the core formation time is reduced by about 3

times from the usual ambipolar diffusion time. Furthermore, the core formation time is considerably reduced when the turbulent speed is larger than the Alfvén speed, i.e., the core formation time is inversely proportional to the square of the turbulent speed.

The equations (15) and (27) are the same as those considered by Mouschovias & Ciolek (1999). Although Mouschovias & Ciolek (1999) considered the static force balance of a subcritical cloud, we showed here that similar relations are applicable to the dynamically oscillating cloud. In addition to the global force balance, a local pressure balance between the magnetic and dynamic pressure is assumed in the dynamically compressible subcritical cloud to obtain the velocity dependence of the ambipolar diffusion time, i.e., the equations (24) and (28). When equation (24) is derived, the relation $B \propto \rho^{1/2}$ is used in the turbulent flows assuming magnetic flux freezing as in equation (20) and (21). Fatuzzo & Adams (2002) studied ambipolar diffusion with the limit of long-wave fluctuations and suggested that there is no net enhancement of the ambipolar diffusion when the density fluctuation depends on the magnetic field fluctuation as $B \propto \rho^{1/2}$. In our case, however, the diffusion is enhanced even when the relation is satisfied. The difference possibly may come from the fact that Fatuzzo & Adams (2002) used a one-dimensional slab model in which the self-gravitational force does not change during the compression along the magnetic field lines if the surface density is constant. In our two-dimensional slab model, the compression perpendicular to the magnetic field enhances the self-gravitational force as well as the density. Our result essentially demonstrates the same result as that of the “gravitationally driven ambipolar diffusion” discussed in Mouschovias & Ciolek (1999) etc, but the density enhancement along with that of the self-gravity is induced by the large-scale compressive turbulent flows.

We showed that the large-scale turbulence associated with density enhancement is an important factor for the fast core formation in turbulent subcritical clouds. In our analysis, the turbulence whose scale is larger than about $4\pi H_0$, which is about 0.6 pc for typical molecular clouds, is needed to get an effective fast ambipolar diffusion. Although the origin of the turbulence in molecular clouds has not yet been identified, the scale of the energy source of the turbulence is supposed to be larger than $4\pi H_0 \sim 0.6$ pc to realize the fast core formation considered in this paper. By comparison, the small-scale turbulence is also considered to be an important factor for the turbulent diffusion processes. For example, the fast ambipolar diffusion rate in a turbulent medium was studied by Zweibel (2002) to explain low magnetic field strength in dense interstellar gas. Leão et al. (2013) pointed out that the “turbulent reconnection diffusion” is also effective to remove the magnetic flux from subcritical cores. These processes would be more efficient if the energy source of the turbulence in molecular clouds is originated in smaller scales. Since the large-scale turbulent flows even in two- or three-dimensional spaces tend to compress the cloud in a one-dimensional manner to make filamentary structures, as seen in Basu et al. (2009) and

Kudoh & Basu (2011), our results can explain generally how core formation is accelerated by the nonlinear large-scale turbulent flows in subcritical magnetic clouds. The results obtained in this paper would be applicable to a filamentary molecular cloud (André et al. 2010) if it is created by a large-scale compression (Peretto et al. 2012). Once the filamentary structure becomes supercritical by the accelerated ambipolar diffusion, the fragmentation along the filament would occur on a dynamical timescale to produce several cores.

When v_{max} is much smaller than the the Alfvén speed, figure 8 shows that the equation (24) does not fit to the numerical results well. This comes from the fact that the equation (15) also does not fit to the numerical results well in figure 9, when the density peak is small. When the density peak is very small, the assumption of the force balance between gravity and magnetic force for the density peak, which is used to derive equation (15), may not be acceptable. Thus, the formula may not be well applied to the quasi-linear regime of the compression, although it is applicable to the nonlinear regime in which we are mostly interested in this paper. When v_{max} is much greater than the Alfvén speed, the collapse may happen more quickly during the compression. If the flow speed is large enough that vertical hydrostatic equilibrium along the magnetic field cannot be attained, then $\rho \propto \Sigma \propto L^{-1}$ and $\tau_{AD} \propto L^{5/2} \propto \rho^{-5/2}$ (Elmegreen 2007; Kudoh & Basu 2008). (The scaling law of τ_{AD} is derived from equation (31) by using $H \sim H_0$.) In this case, the ambipolar diffusion can occur more quickly when the compression leads to large values of ρ . This process would be happening for $t/t_0 < 1$ even in our results, although the overall timescale of the core formation is dominated by the time after the vertical hydrostatic equilibrium is reestablished. The simulation with greater v_{max} was not successful in our case because the density after the first compression becomes so great that the simulation does not have enough spatial resolution for the high density self-gravitating cores. Adaptive mesh refinement or nested grid techniques might be needed for the further investigation in the case of greater v_{max} . However, the turbulent flows in molecular clouds are observed to not be highly super Alfvénic (see the fit to data in Basu (2000)). The parameters we used in this paper can be considered to be within a proper range for typical molecular clouds.

In the case of $\beta_0 = 0.04$, in figure 8, the core formation time seems to be slightly smaller than what is expected from the semi-analytic formula. This may be caused by the fact that the approximation of flux-freezing during the compression, which is used in equation (20), is not a good approximation when the parameter β_0 is small. The local ambipolar diffusion time (τ_{AD}) is estimated to be

$$\tau_{AD} \sim \frac{4\pi}{\gamma} \frac{L^2 \rho^{3/2}}{B^2} \quad (29)$$

$$\sim \frac{4\pi}{\gamma} \frac{H_0^2 \rho_0^{3/2}}{B_0^2} \left(\frac{L}{H} \right)^2 \left(\frac{\rho}{\rho_0} \right)^{-1/2} \quad (30)$$

$$\sim \frac{1}{2\gamma\sqrt{2\pi G}}\beta_0\left(\frac{L}{H}\right)^2\left(\frac{\rho}{\rho_0}\right)^{-1/2}t_0, \quad (31)$$

when we use equation (20). When $\beta_0 \simeq 0.04$, $L \sim 2\pi H$ and $\rho \sim 10\rho_0$, we can get $\tau_{AD} \sim 2t_0$. This means that the local ambipolar diffusion time after the compression becomes nearly comparable to the compression time when $\beta_0 = 0.04$. If the local ambipolar diffusion time is comparable to the compression time, the density can be much more enhanced than estimated from equation (22) for the same velocity because the magnetic pressure after the compression is reduced by the diffusion. This density enhancement leads to a smaller core formation time through equation (15) that seems to be satisfied even in the case of $\beta_0 = 0.04$ from Figure 9. The parameter $\beta_0 = 0.04$ corresponds to $\mu_S = 0.2$. The case of even lesser initial mass-to-flux ratio may result in a shorter core formation time than is estimated from equation (15). This should be confirmed in the future, and will require greater spatial resolution because a stronger magnetic field generally requires greater density near the core center before the onset of runaway collapse.

From Table 1 and Figure 7, the dimensional core formation time is estimated to be about 2×10^6 year, when the flow speed in the cloud is 10 times greater than the sound speed, in the case that the initial mass-to-flux ratio is about half of the critical value (i.e., $\beta_0 = 0.25$). This core formation time is consistent with those of the previous three-dimensional simulations with turbulent flows (Kudoh & Basu 2011), although the core formation time of the present simulation is slightly longer than that of the three-dimensional simulation with the same initial flow speed. This is because that the flow speeds in the three dimensional simulations were the averages of the turbulent flows, and the flow components with speeds greater than the average could slightly shorten the core formation times. In both cases, our simulations show that the core formation time is estimated to be the order of a few to several $\times 10^6$ years for the subcritical molecular clouds whose initial mass-to-flux ratios are about half of the critical value given that initial large-scale flow speeds (whether they are turbulent or not) are 3 – 10 times greater than the sound speed.

Numerical simulations were performed on the SX-9 and on the PC cluster at the Center for Computational Astrophysics in National Astronomical Observatory of Japan. S.B. is supported by a Discovery Grant from the Natural Sciences and Engineering Research Council (NSERC) of Canada.

REFERENCES

Alves, F. O., Franco, G. A. P., & Girart, J. M. 2008, *A&A*, 486, L13

- André, Ph. et al., 2010, *A&A*, 518, L102
- Basu, S. 2000, *ApJ*, 540, L103
- Basu, S., & Mouschovias, T. Ch. 1994, *ApJ*, 432, 720
- Basu, S., & Ciolek, G. E. 2004, *ApJ*, 607, L39
- Basu, S., Ciolek, G. E., Dapp, W. B., & Wurster, J. 2009, *NewA*, 14, 483
- Ciolek, G. E., & Basu, S. 2006, *ApJ*, 652, 442
- Cortes, P. C., Crutcher, R. M., & Watson, W. D. 2005, *ApJ*, 628, 780
- Crutcher, R. M., Hakobian, N., & Troland, T. H. 2009, *ApJ*, 692, 844
- Elmegreen, B. G. 2007, *ApJ*, 668, 1064
- Heyer, M., Gong, H., Ostriker, E., & Brunt, C. 2008, *ApJ*, 680, 420
- Fatuzzo, M., Adams, F. C. 2002, *ApJ*, 570, 210
- Indebetouw, R. M., & Zweibel, E. G. 2000, *ApJ*, 532, 361
- Jijina, J., Myers, P. C., & Adams, F. C. 1999, *ApJS*, 125, 161
- Kudoh, T., & Basu, S. 2003, *ApJ*, 595, 842
- Kudoh, T., & Basu, S. 2006, *ApJ*, 642, 270
- Kudoh, T., Basu, S., Ogata, Y., & Yabe, T. 2007, *MNRAS*, 380, 499
- Kudoh, T., & Basu, S. 2008, *ApJ*, 679, L97
- Kudoh, T., & Basu, S. 2011, *ApJ*, 728, 123
- Langer, W. D. 1978, *ApJ*, 225, 95
- Leão, M. R., de Gouveia Dal Pino, E. M., Santos-Lima, R., & Lazarian, A. 2013, *ApJ*, 777, 46
- Li, H.-B., Dowell, C. D., Goodman, A., Hildebrand, R., & Novak, G. 2009, *ApJ*, 704, 891
- Li, Z.-Y., & Nakamura, F. 2004, *ApJ*, 609, L83
- McKee, C. F., & Ostriker, E. C. 2007, *ARAA*, 45, 565

- Miyama, S. M., Narita, S., & Hayashi, C. 1987a, *Prog. Theor. Phys.*, 78, 1051
- Miyama, S. M., Narita, S., & Hayashi, C. 1987b, *Prog. Theor. Phys.*, 78, 1273
- Mouschovias, T. Ch. 1978, in *Protostars and Planets*, ed. Gehrels, T., Univ. of Arizona Press:Tucson, 209
- Mouschovias, T. Ch., & Ciolek, G. E. 1999, *The Origin of Stars and Planetary Systems*, ed. Lada, C. J. & Kylafis N. D., Kluwer:Dordrecht, 305
- Mouschovias, T. Ch., & Tassis, K. 2009, *MNRAS*, 400, 15
- Ogata, Y., Yabe, T., Shibata, K., & Kudoh, T. 2004, *International Journal of Computational Methods*, 1, 201
- Peretto, N. et al., 2012, *A&A*, 541, 63
- Shu F. H., Adams, F. C., Lizano, S. 1987, *ARA&A*, 25, 23
- Spitzer, L. Jr. 1942, *ApJ*, 95, 329
- Zweibel, E. G. 1998, *ApJ*, 499, 746
- Zweibel, E. G. 2002, *ApJ*, 567, 962

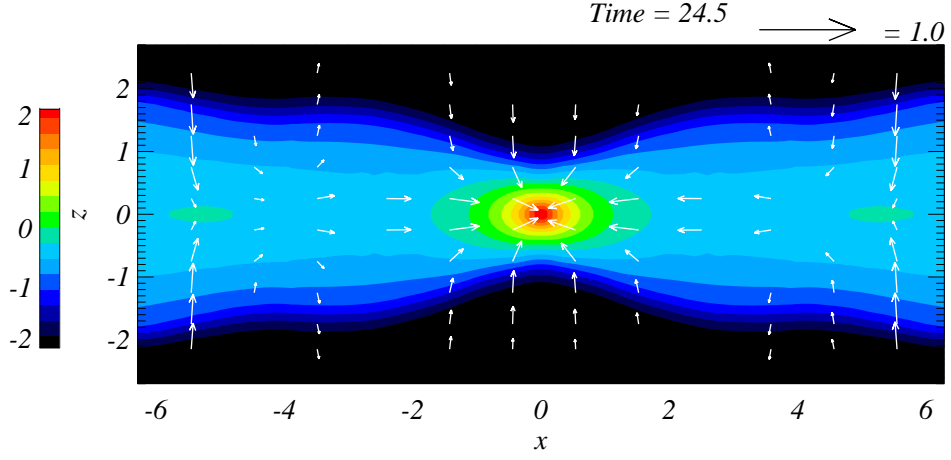


Fig. 1.— Logarithmic density contours at $t/t_0 = 24.5$ for model A5. Arrows show velocity vectors.

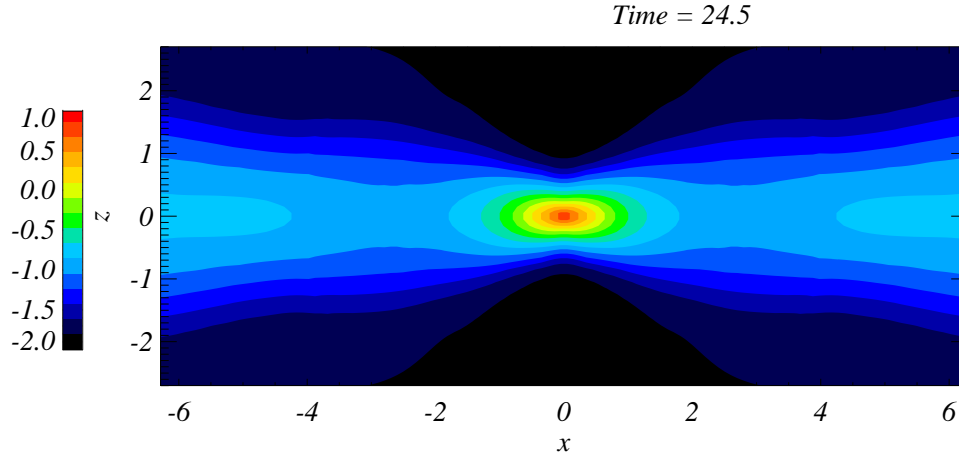


Fig. 2.— Logarithmic plasma β at $t/t_0 = 24.5$ for model A5.

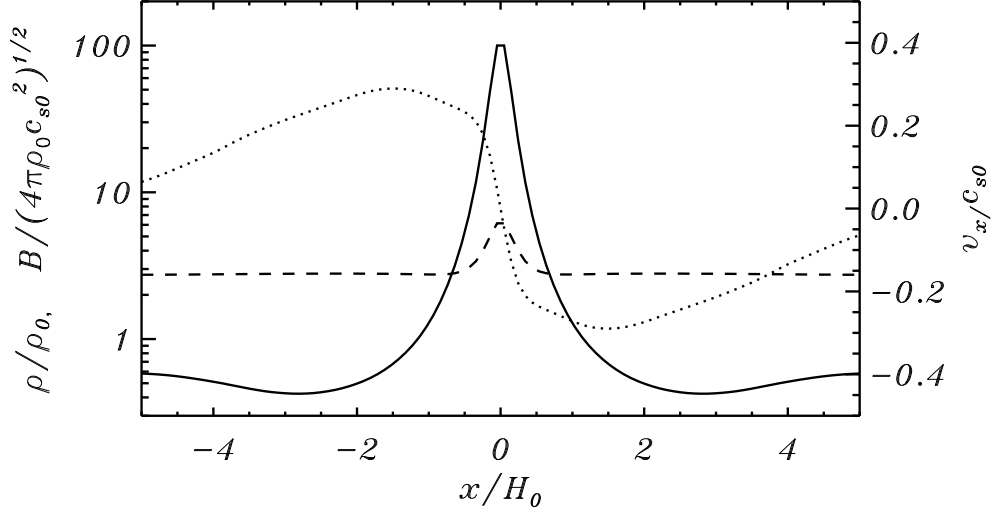


Fig. 3.— Spatial profiles of density (the solid line), strength of magnetic field (the dashed line), and x-velocity (the dotted line) along x on $z = 0$ for model A5 at $t/t_0 = 24.5$.

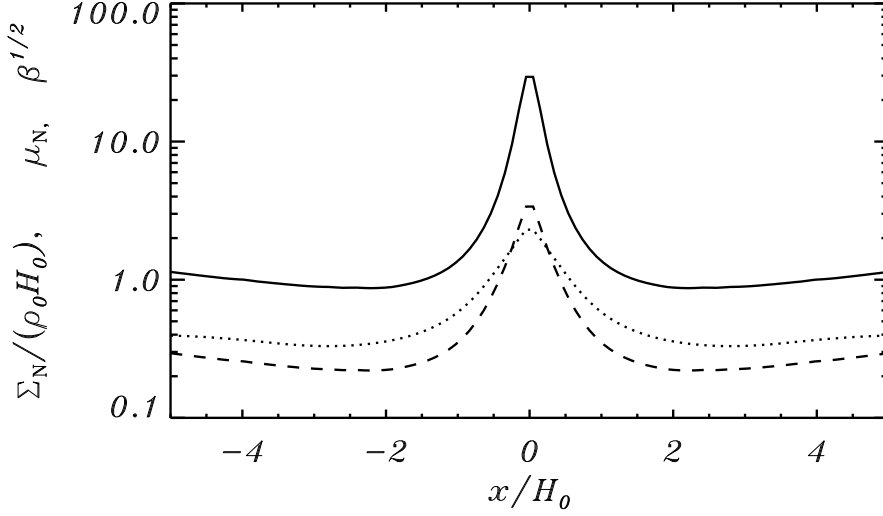


Fig. 4.— Spatial profiles of surface density (the solid line), and normalized mass-to-flux ratio (μ_N : the dashed line) along x for model A5 at $t/t_0 = 24.5$. The square root of plasma β (the dotted line) along x on $z = 0$ is also plotted.

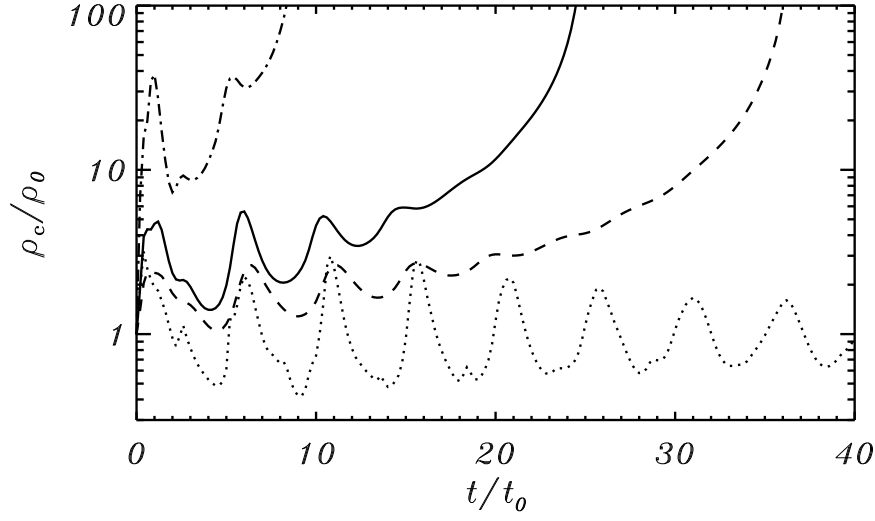


Fig. 5.— Time evolution of the density at $x = z = 0$ (ρ_c). The solid line shows the case of model A5. The dashed lines show the case of model A3, and the dotted-dashed lines show the case of model A10. The dotted lines shows the case of model E5 in which the parameters are the same as those of model A5 except that the ambipolar diffusion is switched off.

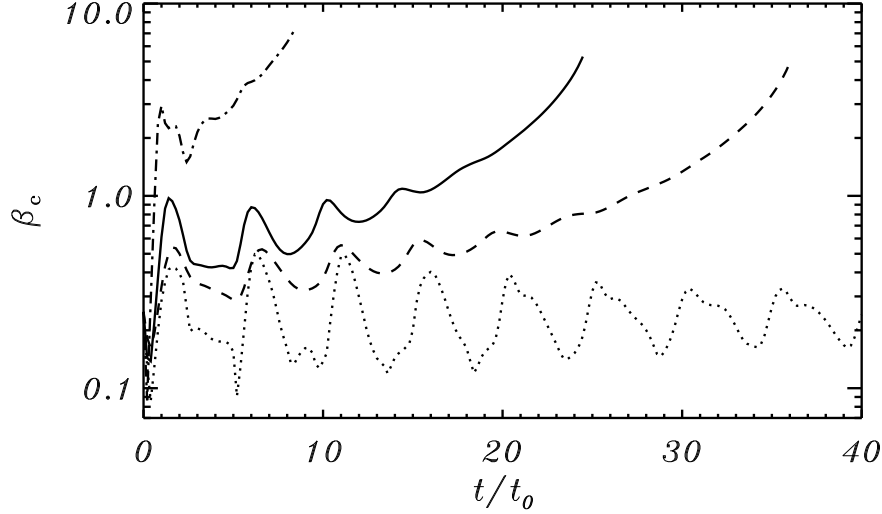


Fig. 6.— Time evolution of the plasma β at $x = z = 0$ (β_c). The solid line shows the case of model A5. The dashed lines show the case of model A3, and the dotted-dashed lines show the case of model A10. The dotted lines shows the case of model E5 in which the parameters are the same as those of model A5 except that the ambipolar diffusion is switched off.

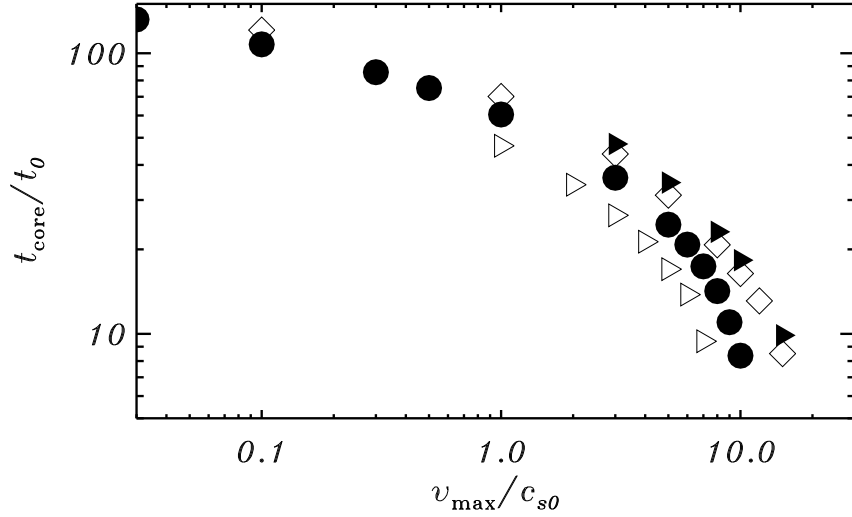


Fig. 7.— Core formation time as a function of initial amplitude of flow speed normalized by the sound speed in the clouds. The filled circles show the case of $\beta_0 = 0.25$. The open squares show the case of $\beta_0 = 0.09$. The open triangles show the case of $\beta_0 = 0.49$. The filled triangles show the case of $\beta_0 = 0.04$.

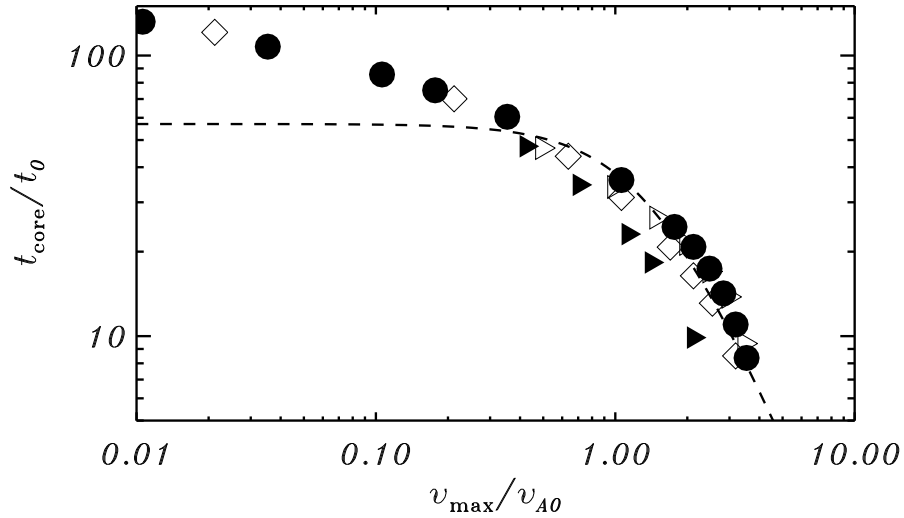


Fig. 8.— Core formation time as a function of initial amplitude of flow speed normalized by initial Alfvén speeds on the midplanes in clouds. The filled circles show the case of $\beta_0 = 0.25$. The open squares show the case of $\beta_0 = 0.09$. The open triangles show the case of $\beta_0 = 0.49$. The filled triangles show the case of $\beta_0 = 0.04$. The dashed line is drawn from equation (24), using $v_{t0} \sim 0.5v_{max}$ as an average speed.

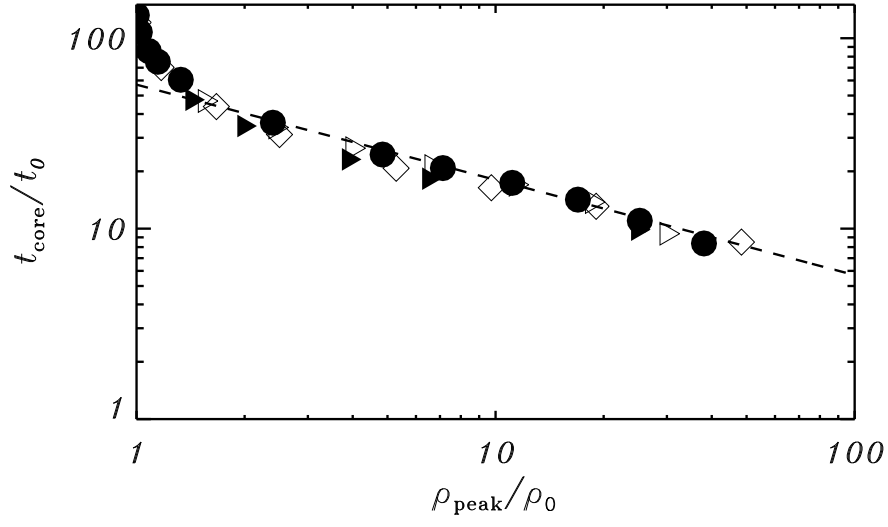


Fig. 9.— Core formation time as a function of the density peak (ρ_{peak}) during the first compression in its time evolution. The filled circles show the case of $\beta_0 = 0.25$. The open squares show the case of $\beta_0 = 0.09$. The open triangles show the case of $\beta_0 = 0.49$. The filled triangles show the case of $\beta_0 = 0.04$. The dashed line is drawn from equation (15), using $\rho \sim \rho_{\text{peak}}$.

Table 1. Model and Parameters

Model	β_0	v_{max}/c_{s0}	v_{max}/v_{A0}	t_{core}/t_0	notes
A003	0.25	0.03	0.011	132	
A01	0.25	0.1	0.035	108	
A03	0.25	0.3	0.11	85.6	
A05	0.25	0.5	0.18	75.2	
A1	0.25	1.0	0.35	60.5	
A3	0.25	3.0	1.1	36.0	
A5	0.25	5.0	1.8	24.5	
A6	0.25	6.0	2.1	20.8	
A7	0.25	7.0	2.5	17.4	
A8	0.25	8.0	2.8	14.2	
A9	0.25	9.0	3.2	11.0	
A10	0.25	10.0	3.5	8.36	
B01	0.09	0.1	0.021	121	
B1	0.09	1.0	0.21	70.1	
B3	0.09	3.0	0.64	43.8	
B5	0.09	5.0	1.1	31.2	
B8	0.09	8.0	1.7	20.8	
B10	0.09	10.0	2.1	16.4	
B12	0.09	12.0	2.5	13.1	
B15	0.09	15.0	3.2	8.50	
C1	0.49	1.0	0.50	46.8	
C2	0.49	2.0	1.0	34.0	
C3	0.49	3.0	1.5	26.5	
C4	0.49	4.0	2.0	21.3	
C5	0.49	5.0	2.5	17.0	
C6	0.49	6.0	3.0	13.8	
C7	0.49	7.0	3.5	9.41	
D3	0.04	3.0	0.42	47.5	
D5	0.04	5.0	0.71	34.6	
D8	0.04	8.0	1.1	23.1	
D10	0.04	10.0	1.4	18.3	
D15	0.04	15.0	2.1	9.88	
E5	0.25	5.0	1.8	–	no ambipolar diffusion

Note. — β_0 is the initial plasma β at $z = 0$, which represents the square of initial mass-to-flux ratio (see equation (7)). v_{max} is the amplitude of the initial velocity fluctuation. t_{core} is the time of collapsing core formation. c_{s0} and v_{A0} are initial sound and Alfvén speeds, respectively.